An Assessment of Weather Analysis Data for the DSN Sites

David D. Morabito,* Longtao Wu,† and Joaquim Teixeira.†

ABSTRACT. — We examine twenty years of weather analysis data (WDA) acquired from the Deep Space Network (DSN) sites as well as the European Centre for Medium-Range Weather Forecasts (ECMWF) fifth generation ECMWF atmospheric reanalysis (ERA5) data referenced to those sites spanning from 2001 to 2020. Annual and seasonal statistics of atmospheric attenuation and atmospheric noise temperature were estimated from the data using the established model formulation of the Radiocommunication Sector of the International Telecommunications Union (ITU-R). We also conducted comparisons of these statistics with those extracted from water vapor radiometers (WVR) that reside or have resided at the sites for overlapping years. This article attempts to characterize the statistical behavior of the extracted atmospheric attenuation and atmospheric noise temperature over a 20-year period. We find that the data types show no significant trends within the 20-year period and that there are some site-dependent differences in the statistics with respect to those of other data sources (e.g., WVR, ITU). These data sets were developed as alternatives to ones used in the machine learning (ML) forecast models.

I. Introduction

In this study, we made use of surface meteorological data as well as fifth-generation European Centre for Medium-Range Weather Forecasts (ECMWF) atmospheric reanalysis (ERA5) data of the global climate to extract contributions of atmospheric attenuation and atmospheric noise temperature used in spaceflight link budget analyses. The resulting statistics were generated for use at frequency bands allocated for deep space communications such as Ka-band (32 GHz) [1], where atmospheric degradation to the received and transmitted signals is a concern.

A previous article [2] provided details on a comparison of calculated atmospheric effects using different methods involving weather data from the Deep Space Network (DSN) sites and two Near Earth Network (NEN) sites commonly used in telecommunications links. Here, we compare atmospheric attenuation estimated from International Telecommunication Union (ITU) models against those derived from water vapor

* Communications Architectures and Research Section.

† Mission Systems and Operations Section.

The research described in this publication was carried out by the Jet Propulsion Laboratory, California Institute of Technology, under a contract with the National Aeronautics and Space Administration.

radiometer (WVR) measurements at the three DSN sites and found them to be in reasonable agreement. We believed a few discrepancies to be consistent with higher uncertainties in the ITU models or their inputs, especially with the liquid content models (rain and clouds) at higher percentiles. The DSN attenuation statistics we derived from WVRs provided a good testbed in which to cross-compare against the statistics of atmospheric losses derived from ITU prediction methods.

Another study compared atmospheric data-type statistics derived from advanced WVR (AWVR) data against ITU models, covering the years from 2001 to 2015 [3]. Other related studies involved a comparison of atmospheric quantities derived from AWVRs and weather analysis data [4].

In a more recent study, we examined and cross-compared statistics and time-variability of the AWVR brightness temperatures and of meteorological data types extracted from AWVR measurements acquired during 2001–2021 at Goldstone, California [5]. The calibrated/validated AWVR data in this study were used as training and testing data sets in an ML forecast system designed to predict atmospheric noise temperature (T_{atm}) at DSN tracking sites in support of deep space missions [6]. Here, the addition of Goldstone AWVR data from 2016 to 2020 were used in the testing and training of the model. The forecasting model is trained with the National Center for Environmental Prediction (NCEP) forecast and analysis data sets involving the atmospheric noise temperatures derived from on-site AWVRs. Prediction of T_{atm} can be provided up to 16 days ahead.

In this paper, we will discuss the weather data used in the study (Section II); the models used in the analysis, cloud liquid (Section III.A), rain liquid (Section III.B), gaseous absorption (Section III.C), and attenuation to noise temperature conversion formulation (Section III.D); the results achieved for Goldstone (Section IV.A), Madrid (Section IV.B), and Canberra (Section IV.C); and concluding remarks (Section V).

II. The Weather Data

Data used in this study were acquired from meteorological sensors from the three DSN sites as well as from the ERA5 data [7]. The ERA5 data sets were derived from a global numerical weather model with some constraints from satellite and other observations (such as soundings). The ERA5 data sets consist of a large number of hourly estimates of atmospheric, land, and oceanic climate variables, and covers the Earth on a 30-km grid, resolving the atmosphere over 137 levels spanning from the surface up to 80 km. The variables that were used in this study included column-integrated water vapor content (kg/m^2), cloud liquid (kg/m^2), cloud ice water (kg/m^2), rainwater (kg/m^2), and total precipitation (m/hr).

Table 1 lists the locations of the DSN sites used to reference the WDA parameters at zenith. These include longitude, latitude, and geopotential height. The surface weather data (pressure, air temperature, and humidity) from on-site instruments were sampled at one-minute intervals. For some of the analyses, the surface weather data were averaged in one-hour segments to be consistent with the one-hour sampling with that of the ML-hourly data sets.

Table 1. Deep Space Network Site Locations

DSN Site	Longitude (deg East)	Latitude (deg)	HMSL (m)
Goldstone	243.126	35.24	919
Madrid	355.750	40.24	619
Canberra	148.980	–35.20	676

HMSL: Height above mean sea level

We make use of ITU-R models (to be discussed in Section III) to convert the meteorological measurements to signal attenuation. This involves estimating attenuation contributions due to cloud liquid, rain liquid, and atmospheric gases of oxygen and water vapor. For this study, we assumed that scintillation was negligible for the elevation angles applicable to the DSN and the frequencies of interest. In previous studies, scintillation was measured to be ~0.2 dB (and below) at very low elevation angles (~14 deg) and at Ka-band (32 GHz) frequencies at the Goldstone site [8], which is significantly below the level of atmospheric attenuation (~1 dB and higher) expected at these elevation angles for 32 GHz Ka-band.

III. Models

The models discussed below were used to generate time series of the atmospheric attenuation due to clouds, rain, and gas. From these time series, the cumulative distributions (CD) were derived for each year of data. Thus, the CD curves presented elsewhere in this paper for atmospheric attenuation are based on a sum of cloud liquid, rain liquid, and gaseous contributions as summarized below. Note that ERA5 data were used for cloud liquid and rain liquid as there were operational issues with the DSN rain gauge sensors. We sum the three values of atmospheric attenuation to get total attenuation, scaled to the elevation angle of interest. All formulation was evaluated using a Ka-band link frequency of $f = 32$ GHz.

1) Cloud liquid makes use of columnar cloud liquid content from the ERA5 hourly data as input to the ITU-R model for conversion to atmospheric attenuation [9].

2) Rain liquid content makes use of one-hour accumulated total precipitation from the ERA5 hourly data as input to the ITU-R model for conversion to atmospheric attenuation [10].

3) Gaseous attenuation (oxygen and water vapor) makes use of pressure, temperature, and relative humidity from DSN weather sensors averaged in one-hour segments, input to the ITU models for gaseous attenuation [11]. The difference between using gaseous attenuation estimated using DSN weather sensor data versus that using ERA5 data is usually negligible (well below ~0.1 dB).

A. Cloud Liquid Model

Attenuation due to cloud liquid content makes use of the equations found in ITU-R P.840-8, equation 13 in Reference [9]:

$$A_{cloud}(\text{dB}) = \frac{L\, K_l^*(f, 273.15)}{\sin(\theta)}, \tag{1}$$

where L is the total columnar liquid water content (kg/m^2) (from hourly estimates obtained from ERA5), θ is the elevation angle, and $K_l^*(f,T)$ was based on equation 14 in Reference [9]:

$$K_l^* = \frac{0.819(1.9479 \times 10^{-4} f^{2.308} + 2.9424\, f^{0.7436} - 4.9451)}{\varepsilon''(1+\eta^2)} \quad \text{(dB/km)/(g/m}^3\text{)}. \tag{2}$$

For the analysis presented in this paper, we have assumed an elevation angle of 90 deg (zenith), a link frequency (f) of 32.0 GHz, and a liquid water temperature (T) of 273.15 K for Equations (1) and (2) above. The parameters ε'' and η were obtained from the series of equations 3–9 provided in ITU-R P.840-8 in Reference [9].

B. Rain Liquid Model

The rain model accounts for rain liquid and made use of equations recommended in ITU-R P.838-3 in Reference [10].

The specific attenuation can be obtained using the rain rate of interest R (mm/hr) as

$$\gamma_R = k\, R^{\alpha}, \tag{3}$$

where k and α are obtained as shown below (from ITU-R P.838-3), which are a function of frequency (we assume 32.0 GHz) and sets of coefficients obtained from tables 1–4 in Reference [10]. Hourly estimates of the rain rate used in the model were extracted from the ERA5 data sets (see Section II):

$$k = \frac{k_H + k_V + (k_H - k_V)\cos^2(\theta)\cos(2\tau)}{2} \tag{4}$$

$$\alpha = \frac{k_H \alpha_H + k_V \alpha_V + (k_H \alpha_H - k_V \alpha_V)\cos^2(\theta)\cos(2\tau)}{2k}, \tag{5}$$

where k_H and α_H are the coefficients for horizontal polarization, and k_V and α_V are the coefficients for vertical polarization. The values for these coefficients were estimated using appropriate formulation from Reference [10] and we found them to be in reasonable agreement with those provided in table 5 in [10] for a frequency of 32 GHz ($k_H = 0.2778$, $\alpha_H = 0.9302$, $k_V = 0.2646$, and $\alpha_V = 0.8981$). The polarization tilt angle is denoted by τ, where the value of 45° is used for circular polarization, the default for all deep-space links.

Using formulation found in Reference [11], one can estimate the effective path length for the rain rate of interest, L_e.

One can then estimate the attenuation due to rain as

$$A_{rain} = \gamma_R\, L_e. \tag{6}$$

C. Gaseous Absorption Model

Attenuation due to atmospheric gases are due primarily to oxygen (the dry atmosphere), which is fairly stable, and water vapor (the wet atmosphere), which is very variable. The oxygen contribution defines the minimum level of attenuation when the atmosphere is devoid of water vapor. This is on order of ~0.1 dB at zenith for all three DSN sites.

1. Water Vapor Attenuation

The water vapor contribution makes use of the water vapor density, ρ, which can be obtained from the ERA5 data sets or calculated from surface meteorological measurements of pressure, temperature, and relative humidity from nearby weather sensors at the DSN sites, making use of a formulation found in ITU-R P.453-14 in Reference [12].

The water vapor density in gm/m^3 is calculated as

$$\rho = \frac{216.7\, e}{T}, \tag{7}$$

where T is air temperature in K and e is water vapor density given as

$$e \; = RH\; e_s, \tag{8}$$

where RH is relative humidity (0–1) and e_s is saturated vapor density, which for water vapor is

$$e_s = \; EF_{water}\; 6.1121 \exp\left[\frac{\left(18.678 - \frac{T_C}{234.5}\right) T_C}{T_C + 257.14}\right] \tag{9}$$

with

$$EF_{water} = 1 + 0.0001\left[7.2 + P\left\{0.0320 + 5.9 \times 10^{-6}\, {T_C}^2\right\}\right], \tag{10}$$

where P is total (dry + vapor) atmospheric pressure (hPa) and T_C is air temperature in °C.

From line 15 of the text in ITU-R SA.2183 in Reference [11], the specific attenuation at ground level due to water vapor, from sea level up to an altitude of 10 km, at frequency f (in GHz) is given by

$$\begin{aligned}\gamma_w = \Bigg\{ & \frac{3.98\eta_1 \exp[2.23(1-r_t)]}{(f-22.235)^2 + 9.42\eta_1^2} g(f,22) + \frac{11.96\eta_1 \exp[0.7(1-r_t)]}{(f-183.31)^2 + 11.14\eta_1^2} \\ & + \frac{0.081\eta_1 \exp[6.44(1-r_t)]}{(f-321.226)^2 + 6.29\eta_1^2} + \frac{3.66\eta_1 \exp[1.6(1-r_t)]}{(f-325.153)^2 + 9.22\eta_1^2} \\ & + \frac{25.37\eta_1 \exp[1.09(1-r_t)]}{(f-380)^2} + \frac{17.4\eta_1 \exp[1.46(1-r_t)]}{(f-488)^2} \\ & + \frac{844.6\eta_1 \exp[0.17(1-r_t)]}{(f-557)^2} g(f,557) \\ & + \frac{290\eta_1 \exp[0.41(1-r_t)]}{(f-752)^2} g(f,752) \\ & + \frac{8.3328 \times 10^4 \eta_2 \exp[0.99(1-r_t)]}{(f-1\,780)^2} g(f,1\,780) \Bigg\} f^2 r_t^{2.5} \rho \times 10^{-4}\end{aligned} \tag{11}$$

with

$$\eta_1 = 0.955 r_p r_t^{0.68} + 0.006\rho$$

$$\eta_2 = 0.735 r_p r_t^{0.5} + 0.0353 r_t^4 \rho,$$

and

$$g(f, f_i) = 1 + \left(\frac{f - f_i}{f + f_i}\right)^2,$$

where ρ is the water density (g/m^3) at the station location as calculated above in Equation (7),

$$r_t = \frac{288}{273 + T_C},$$

where T_C is air temperature (°C) obtained from surface meteorological data, and

$$r_p = P/1013.$$

Equivalent water vapor height h_w at the Earth station elevation at frequency f is given in Reference [11]:

$$h_w = 1.66\left(1 + \frac{1.39\sigma_w}{(f-22.235)^2 + 2.56\sigma_w} + \frac{3.37\sigma_w}{(f-183.31)^2 + 4.69\sigma_w} + \frac{1.58\sigma_w}{(f-325.1)^2 + 2.89\sigma_w}\right), \tag{12}$$

where

$$\sigma_w = \frac{1.013}{1 + \exp\left[-8.6(r_p - 0.57)\right]}.$$

2. Attenuation Due to Dry Air

The specific attenuation at ground level due to oxygen (dry air), γ_0 in dB/km, at frequency f is given by ITU-R SA.2183 in Reference [11]:

$$\gamma_0 = \left[\frac{7.2r_t^{2.8}}{f^2 + 0.34\, r_p^2\, r_t^{1.6}} + \frac{0.62\xi_3}{(54-f)^{1.16\xi_1} + 0.83\xi_2}\right] f^2 r_p^2 \times 10^{-3} \tag{13}$$

with

$$\xi_1 = \phi(r_p, r_t, 0.0717, -1.8132, 0.0156, -1.6515)$$
$$\xi_2 = \phi(r_p, r_t, 0.5146, -4.6368, -0.1921, -5.7416)$$
$$\xi_3 = \phi(r_p, r_t, 0.3414, -6.5851, 0.2130, -8.5854)$$
$$\phi(r_p, r_t, a, b, c, d) = r_p^a r_t^b \exp[\, c(1 - r_p) + d(1 - r_t)].$$

The equivalent height due to the dry air (oxygen) component of gaseous attenuation (h_o in km) is given by ITU-R SA.2183 in Reference [11]

where

$$h_o = \frac{6.1}{1 + 0.17 r_p^{-1.1}}(1 + t_1 + t_2 + t_3)$$

$$t_1 = \frac{4.64}{1 + 0.066 r_p^{-2.3}} \exp\left[-\left(\frac{f - 59.7}{2.87 + 12.4\exp(-7.9 r_p)}\right)^2\right]$$

$$t_2 = \frac{0.14\exp(2.12 r_p)}{(f - 118.75)^2 + 0.031\exp(2.2 r_p)} \tag{14}$$

$$t_3 = \frac{0.0114}{1 + 0.14 r_p^{-2.6}} f \frac{-0.0247 + 0.0001 f + 1.61 \times 10^{-6} f^2}{1 - 0.0169 f + 4.1 \times 10^{-5} f^2 + 3.2 \times 10^{-7} f^3}$$

$h_o \leq 10.7 r_p^{0.3}$ when $f < 70$ GHz,

where

f = frequency (GHz)

r_p = $p/1013$

p = pressure (hPa) at the station location.

It should be borne in mind that the formulation presented here is intended to be approximate and is not as accurate as the line-by-line formulation presented in ITU-R P.676.12 from Reference [13]. Since the oxygen contribution to overall attenuation and noise temperature increase is small, we can neglect the use of the more rigorous formulation for this contribution, especially as it becomes less significant at the high CD values.

3. Total Gaseous Attenuation

The total attenuation at zenith due to the gaseous contributions at the elevation angle range applicable for the DSN is given by Reference [11] (in dB)

$$A_{gas}(\theta) = \frac{A_O + A_w}{\sin\theta}. \tag{15}$$

For this study, we consider only the elevation angle at zenith (90°), thus

$$A_{gas}(90°) = \gamma_o \; h_o + \gamma_w \; h_w. \tag{16}$$

D. Conversion Formulation Between Atmospheric Attenuation and Atmospheric Noise Temperature

Total attenuation at zenith is thus the sum of the gaseous (Equation (16)), cloud (Equation (1)), and rain (Equation (6)) contributions to the attenuation at zenith (all in dB).

$$A = A_{gas} + A_{cloud} + A_{rain}. \tag{17}$$

Atmospheric attenuation refers to signal strength loss due to the atmosphere and is given by

$$L_{atm}(\theta) = \exp\left[-\left(\frac{\tau_z}{\sin(\theta)}\right)\right], \tag{18}$$

where τ_z is the optical depth at zenith ($\theta = 90°$), which is given as

$$\tau_z = -\ln\left(\frac{T_{phys} - T_{atm}}{T_{phys} - T_{cosmic}}\right), \tag{19}$$

where T_{cosmic} is the unattenuated microwave background temperature (2.725 K), T_{phys} refers to the mean effective radiative temperature of the atmosphere (~280 K; [1]), and T_{atm} represents atmospheric noise temperature (at zenith).

The atmospheric loss factor L_{atm} in (18) can be related to the atmospheric attenuation in dB units (Equation (17)) by

$$A(\theta) = 10\ \log_{10}[L_{atm}(\theta)]. \tag{20}$$

The overall system noise temperature T_{sys} at elevation angle θ is related to noise power in the received signal and is a sum of atmospheric, microwave equipment and cosmic background contributions [14]. One can estimate τ_z from atmospheric attenuation and elevation angle using Equation (18) from which one can estimate the atmospheric noise temperature contribution, T_{atm}, using Equation (19) rewritten as

$$T_{atm}(\theta) = T_{phys}\left[1 - \exp\left[-\left(\frac{\tau_z}{sin(\theta)}\right)\right]\right]. \tag{21}$$

Given that we track T_{atm} statistics such as specified in the DSN documentation [1], flight projects typically design their links using conservative values of cumulative distribution, most predominately 90% or 95%.

IV. Results

The models in Section III were used to generate time series of the atmospheric attenuation due to gas, clouds, and rain. From these time series, the cumulative distributions were derived for each year. We then evaluated the statistics of atmospheric attenuation for each DSN site, which are presented here. These statistics are also compared with those provided in the DSN 810-005 documentation [1] used by flight projects to account for atmospheric effects in their link analyses.

A. Goldstone

Plots of attenuation cumulative distribution are shown in Figure 1. For years 2009–2020 (Figure 1a), we made use of weather data obtained from instruments of the weather station designated Deep Space 24 (DS24), which resides in the Apollo Valley at Goldstone, which is where the Ka-band equipped beam waveguide (BWG) antenna Deep Space Station 25 (DSS-25) is located. We see from Figure 1a that the CD curves (solid colors) are in reasonable agreement to within a few 0.01 dB of the DSN Telecommunications Link

Design Handbook CD curve [1] (dashed black), but biased slightly to the left at intermediate CD values. Given that the nearby weather station at the Apollo Valley subcomplex (designated DS24) did not come up online until June 25, 2009, we made use of weather data acquired from another Goldstone site (designated DS10), located several km away from the Apollo Valley DS24 weather station. The resulting CD curves obtained from DS10 are shown in Figure 1b. Here we see more of a leftward bias of the CD curves relative to the black dashed 810-005 curve. We suspect that the difference may be due to the application of the gaseous attenuation model, or its inputs for the DS10 weather tower site data at low CD values, and some issues with the cloud/rain models (or inputs) at higher CD values. With regards to the gaseous absorption model, the formulation we chose to use is not as accurate as other formulations but was deemed convenient for our purposes (see Section III.C.2).

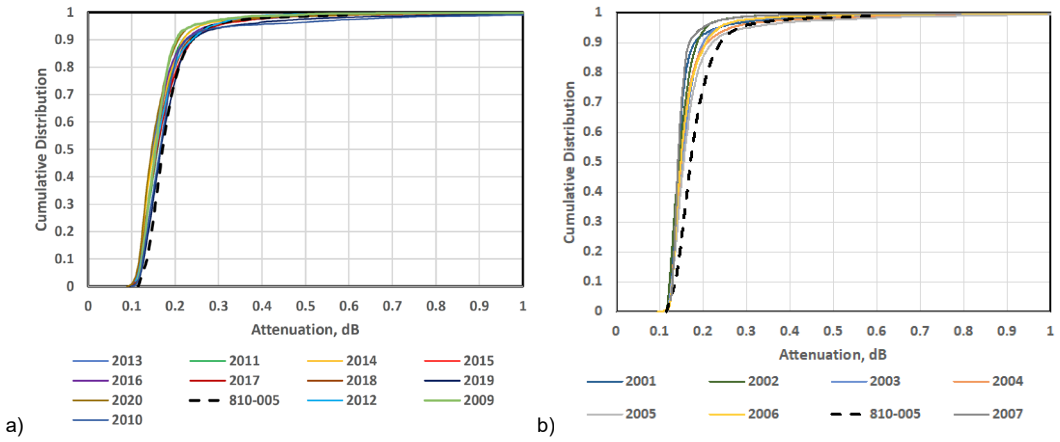

Figure 1. CD curves of atmospheric attenuation a) for 2009–2020 from DS24 weather station (near 34-m DSS-25) and ERA5 data, and b) for 2001–2007 from DS10 weather station (near 70-m DSS-14) and ERA5 data.

If we examine the minimum and median atmospheric attenuation values for each year and compare against the 810-005 values, we get the following results shown in Figure 2. The AWVR median values (green triangles) are in reasonable agreement with the 810-005 median (solid red line), where the average of the AWVR median values is 0.166 dB compared to 0.171 dB 810-005 median (good agreement). The AWVR minimum values (purple triangles) are in reasonable agreement with the 810-005 value (solid blue line), where the average of the AWVR minimum values is 0.102 dB compared to 0.116 dB 810-005 minimum (good agreement). This agreement is expected as the 810-005 statistics were generated from much of the AWVR data.

The WDA median values (red circles) are in reasonable agreement with the 810-005 value (solid red line) but biased upward about ~0.015 dB, where the average of the WDA median values is 0.184 dB compared to the 0.171 dB value from the 810-005 median (good agreement). The WDA minimum values (blue circles) are in reasonable agreement with the 810-005 value (solid blue line), but generally biased upward such as from 2009–2020, where the average of the WDA minimum values is 0.132 dB compared to 0.116 dB minimum from the 810-005 (good agreement). Such agreement between WDA and AWVR/810-005 values are encouraging since discrepancies are expected between on-site AWVR measurements and additional input data sources for WDA, as well as uncertainties

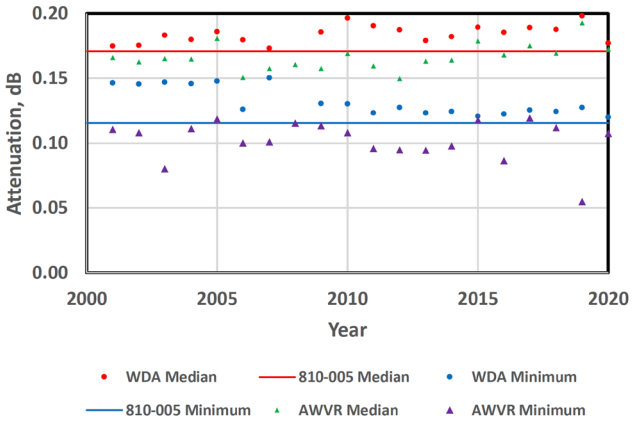

Figure 2. Comparison of yearly estimates of atmospheric attenuation from WDA, AWVR, and 810-005.

in the ITU-R models. However, the ~0.02 dB difference is very small and provides confidence in the results.

We also examined the 95% CD values of atmospheric attenuation. As can be seen in Figure 3, the AWVR values (green circles) are distributed reasonably well against the 810-005 value (solid red line), where the average of the AWVR 95% values is 0.292 dB and that from 810-005 is 0.281 dB. The WDA values (blue circles) have an average value of 0.296 dB, which lies ~0.015 dB above the 810-005 value of 0.281 dB. The fact that the biases in the WDA results are generally largest at intermediate CD values suggests a possible issue in the cloud liquid data or model or the differences may lie within their uncertainties.

Given the consistent ~0.02 dB bias we observed in the above comparisons of the WDA results with the 810-005 model, we performed spot checks with the Slobin model [15]. It was found that the oxygen absorption of the known ITU-R model used (Section III.C.2) was low by 0.02 dB. We thus applied this correction across-the-board to the atmospheric attenuation data and evaluated the resulting atmospheric noise temperature increase using the Section III.D formulation. We then examined the corresponding atmospheric noise temperature statistics for Goldstone. Figure 4 displays the CD curves for the T_{atm}. We see reasonable agreement at low CD values and large differences up to about ~4 K at 95% CD, possibly due to deficiency in the cloud/rain models (and/or inputs) or atmospheric variability. The median T_{atm} values agree well and tend to fall within 1 K of the 810-005 model (see Figure 5). The minimum T_{atm} values tend to agree very well with the 810-005 model for years 2006 and 2009–2020. The minimum values lie ~1 K higher than the 810-005 model for years 2001–2007, except for 2006 (see Figure 6). This difference may be attributable to the different weather instrumentation used, as the weather station for the 2001–2007 data is located several km away from that used for the 2009–2020 data at the Goldstone complex. Another contributing feature was found to be a different minimum response on some of the sensors during the hotter summer months. We note that these ~1 K excursions above the accepted 810-005 value are not critical in the context of accepted ~1–2 K errors in the T_{atm} either through calibration issues or natural variability and given that the values at higher CDs are more pertinent.

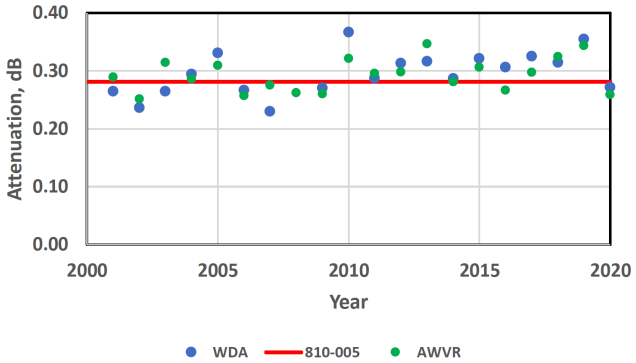

Figure 3. Atmospheric attenuation at a CD of 95% for Goldstone.

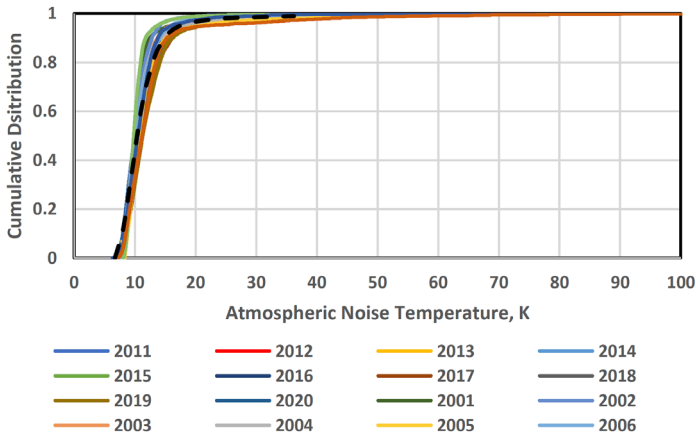

Figure 4. Atmospheric noise temperature cumulative distributions for Goldstone; individual annual averages (solid colors) and 810-005 (dashed black).

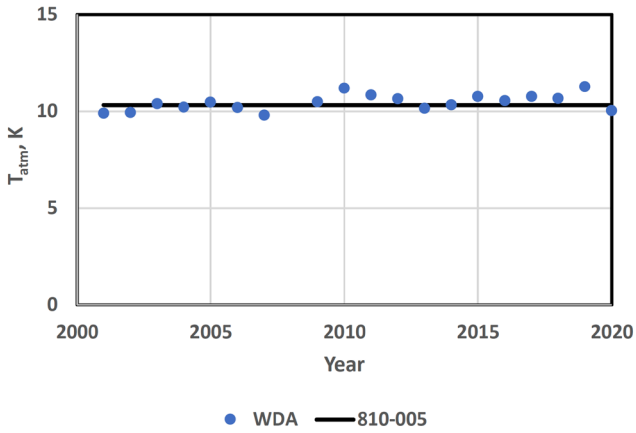

Figure 5. Median T_{atm} values for each year (blue points) and 810-005 model (solid black).

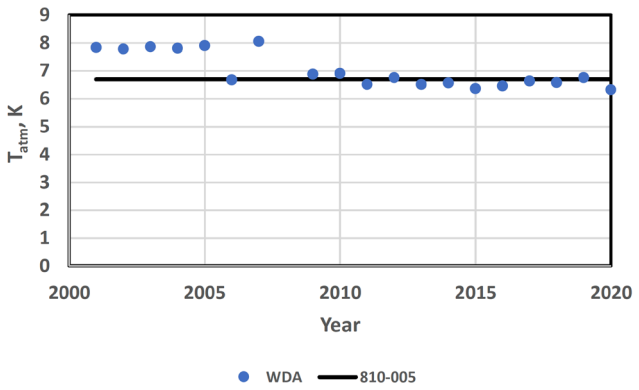

Figure 6. Minimum T_{atm} values for each year (blue points) and 810-005 model (solid black).

B. Madrid

Figure 7 displays the annual cumulative distributions of Ka-band (32 GHz) zenith atmospheric attenuation for years 2006–2020, which were extracted from the weather data analysis involving Section III models (solid colors) and from 810-005 (dashed black) [1]. The cloud water data (dominant at intermediate CD values) apparently does a good job in allowing the CD curve to align with the WVR-based 810-005 curve up to the 90% level despite its large uncertainty.

Atmospheric noise temperature increase can be estimated from atmospheric attenuation using well-known radiative transfer formulation, for CDs on order of 99% and below for most sites (neglecting scattering). In Section II, we discussed the conversion from atmospheric attenuation to atmospheric noise temperature increase.

We conducted an analysis to compare annual zenith noise temperature CDs for both WDA and AWVR data during common years 2004–2015. The comparisons were generally excellent with some small differences noted. Figures 8 and 9 display intercomparisons of

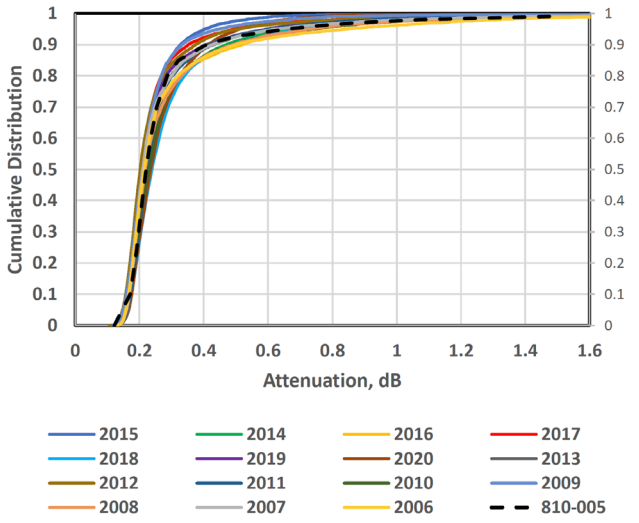

Figure 7. Annual cumulative distribution curves of atmospheric attenuation at Madrid acquired for 2006 through 2020 (solid colors) and 810-005 (dashed black).

atmospheric noise temperature CDs obtained from WDA and AWVR for years 2009 and 2012 when AWVR data were available for Madrid. Figure 8 displays these CD curves where formulation using rain rates as input were used for the WDA, and Figure 9 displays these where formulation with cumulative rainwater as input was used for the WDA data. Statistical rain models typically involve a model using a statistical 0.01% rain rate for a given site as input; however, we used actual rain rates available from the ERA5 data.

One can see generally good agreement with some small differences noted. For instance, for the rain rate formulation, one can see a slight elbow in the 2012 plot (Figure 8b) at CDs near 90%, while the two curves overlay each other nicely for 2009 (Figure 8a). For the case of cumulative rainwater formulation, one can see the WDA curve start to slightly diverge to the left with respect to the AWVR curve above 90% for 2009 (Figure 9a) at CDs above 90%, while the two curves overlay each other nicely for 2012 (Figure 9b).

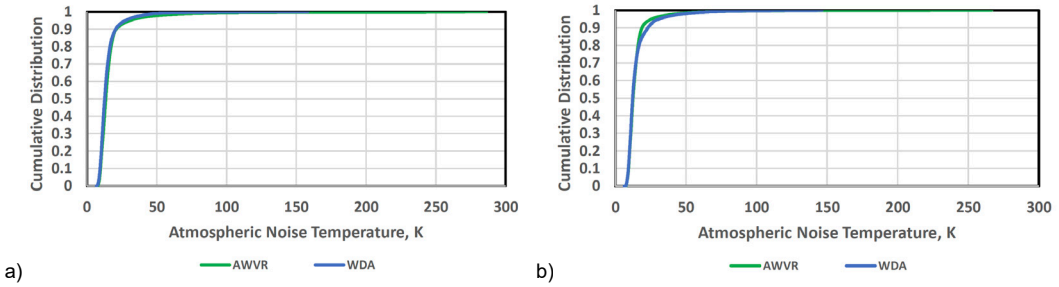

Figure 8. Cumulative distribution of atmospheric noise temperature using rain rate formulation for WDA a) 2009, b) 2012. WDA (blue) AWVR (green).

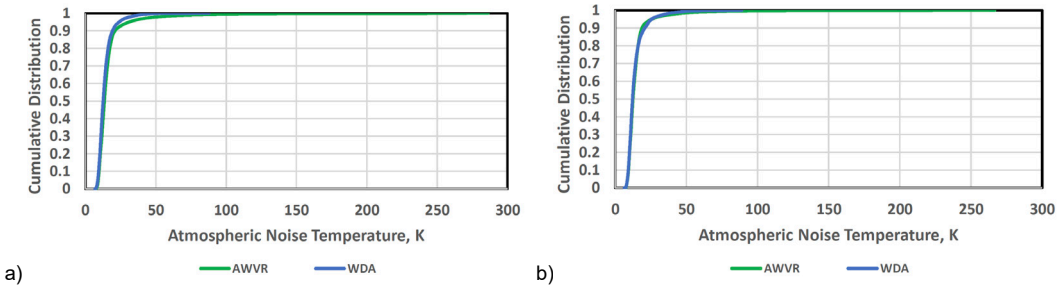

Figure 9. Cumulative distribution of atmospheric noise temperature using cumulative rainwater formulation a) 2009, b) 2012. WDA (blue) AWVR (green).

We performed a comparison of the minimum and median attenuation and T_{atm} values measured for each year of data with AWVR and 810-005. Figure 10 summarizes this comparison for atmospheric attenuation. The differences in the minimum values for each year between AWVR and WDA data sets are usually at ~0.02 dB or below, except for 2015, which was a partial year for the AWVR (purple triangle at 2015). The number of data points for 2015 is almost half of all of the other years, and the selection effect may have been biased toward the warmer months. The minimum values of T_{atm} have agreement within the ~1 K calibration error of AWVR, with each other and with the 810-005 [1] (except for 2015). Again, the AWVR data for 2015 is only for the first half of the year, thus we expect a selection effect due to more humid warmer weather than usual. Figure 11 displays the

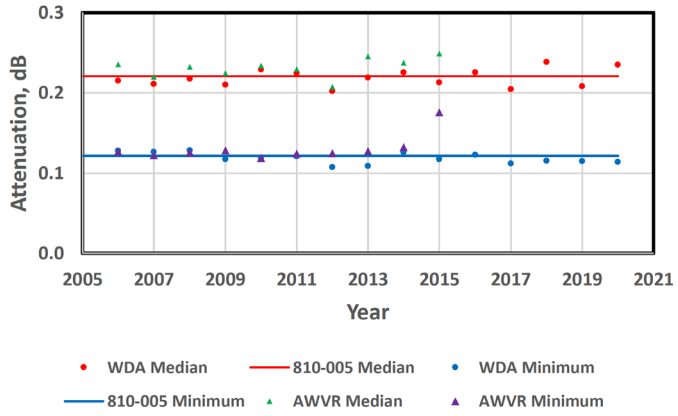

Figure 10. Minimum and median atmospheric attenuation statistics from WDA, AWVR, and 810-005.

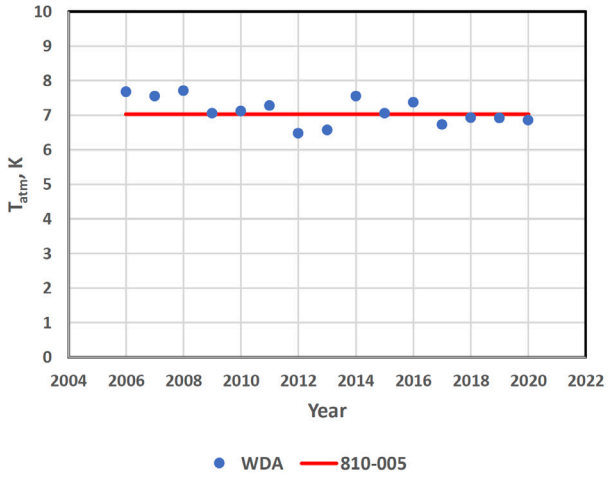

Figure 11. Minimum T_{atm} statistics from WDA (blue points), and 810-005 (solid red).

minimum T_{atm} from WDA for each year where the agreement is very good with the 810-005 minimum for the Madrid site.

We also performed a comparison of the median T_{atm} measurements for each year of data. The differences between AWVR and WDA T_{atm} for each respective year are usually ~1 K or below, except for years 2006, 2013, and 2015 where there may be some selection effects and calibration issues on order of 1 K (known AWVR uncertainty). All median T_{atm}s from the WDA agree within ~1 K of the 810-005 median value (see Figure 12) [1]. This agreement is within the ~1 K calibration error of the AWVR. The worst-case difference between AWVR and WDA T_{atm} is 2.11 K, where selection effects for the 2015 AWVR data set were previously noted.

The maximum values of T_{atm} from AWVR data are in agreement and fall below the maximum physical radiative temperature of the atmosphere (280 K). Most WDA maximum T_{atm}s are much lower than the expected 280 K maximum with differences with AWVR maximum values usually exceeding 100 K (2009–2015). This is possibly explained by the fact that the WDA points are hourly and thus the resulting averages smears out

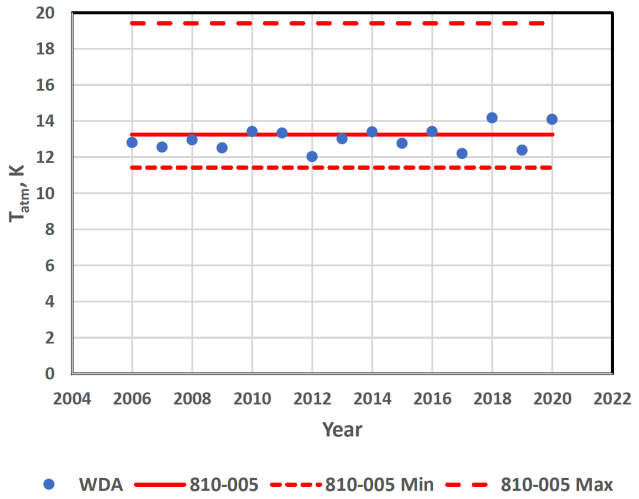

Figure 12. Median T_{atm} statistics from WDA (blue points), and 810-005 (solid red) with minimum and maximum 810-005 medians (dashed lines).

variations involving higher values of T_{atm}, whereas, the AWVR points are sampled at a higher rate, thus capturing more of the high T_{atm} occurrences, which also appear in the CD curves. There are very few points in the data that have T_{atm}s above 200 K, less than say 0.1% of the time, so if averaging does account for this, then this should not be a concern.

C. Canberra

The Canberra WDA results for all available years can be summarized in Figure 13 showing the CD curves of atmospheric attenuation for each of the years from 1999 to 2020 (excluding 2000). The WDA curves (solid colors) cluster close together in reasonable agreement to within ~0.1 dB up to about 50% CD, but many curves lie much further to the right of the referenced 810-005 curve (dashed black) at the higher CDs, suggesting either

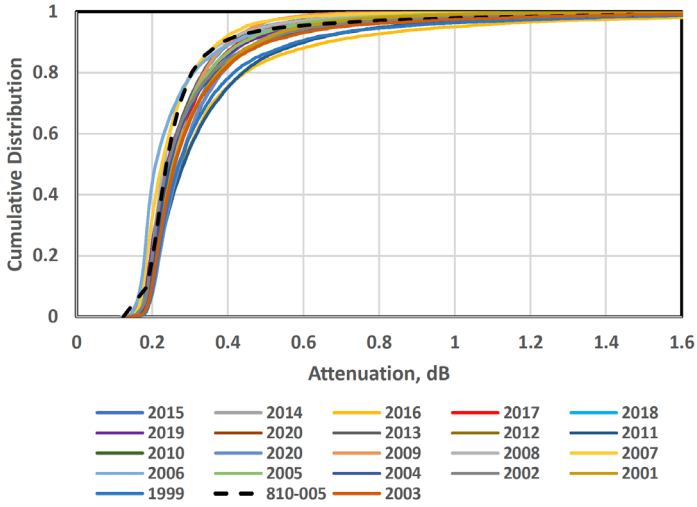

Figure 13. Canberra annual zenith Ka-band atmospheric attenuation cumulative distributions derived from WDA (solid colors) and 810-005 values (dashed black curve).

too much liquid contribution in the weather models or their inputs, or perhaps pointing to an issue with the older model WVR data that generated the 810-005 CD curve, or atmospheric variability, which is deemed unlikely. At 90% CD, the 810-005 curve reaches ~0.4 dB and the eyeballed centroid of the WDA cluster is at ~0.5 dB. This result is consistent with earlier findings from a previous ITU model study where we obtained the same result at 90%, but using a rain rate as input to a statistical model (instead of liquid water content analysis measurements) (see table 18 in [2]). A focus of further study will involve doing a year-by-year comparison of the earlier weather data with the available WVR data results for years that overlap.

Figure 14 displays the CD curves of atmospheric attenuation at the Canberra DSN site for two years in which available WVR data were available and overlapped with the WDA data sets. For both years 1999 (Figure 14a) and 2006 (Figure 14b), there is good agreement between the WVR-derived curves (blue) and the 810-005 curve (dashed black), which is expected since the 810-005 curve was based on the aggregate of available WVR data from Canberra. The WDA curve (red) for 1999 lies significantly to right of the WDA and WVR curves for 1999 (left), but are in better agreement for 2006 (right). By employing a different but independent technique using the ML method including ERA5 data (ERA5 ML), we see that for 1999, the curve (green) still lies significantly to the right of the WVR and 810-005 curves but not as much as the WDA (red) curve. For the year 2006 (Figure 14b), all curves appear to exhibit much better agreement with each other. The ERA5 ML weather forecasting analysis uses five years of ERA5 and WVR data, where four years of data are used to train a random forest (RF) model. The atmospheric noise temperature for the out year can then be estimated using the RF model. A loop is used to create the full data set [6].

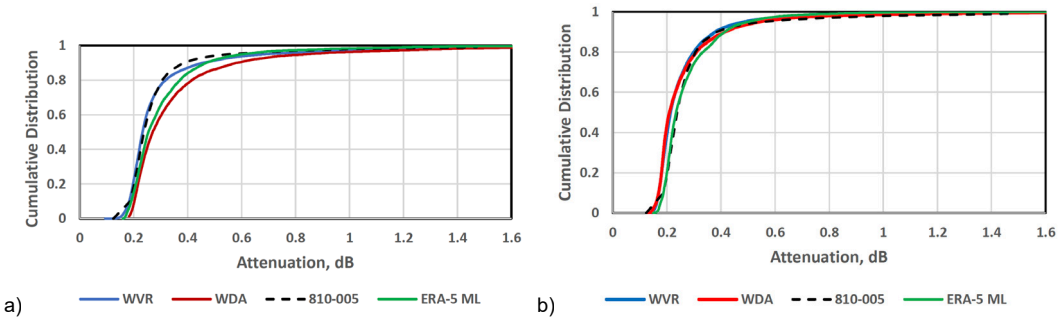

Figure 14. Canberra annual cumulative distribution as a function of atmospheric attenuation for years 1999 (left) and 2006 (right) from WDA (red), WVR (blue), 810-005 (dashed black), and ERA5 ML (green).

Figure 15 displays the median and minimum atmospheric attenuation statistics for the Canberra site based on WDA and WVR measurements along with the 810-005 models. We see generally good agreement between the data sets except for a couple cases of unusually low minimum values from the WVR for years 1999 and 2001 (there was no 2000 WVR data for Canberra). There may have been a WVR calibration problem during 1999 and 2001. The WDA annual values (red data points) tend to be biased somewhat higher than the 810-005 median (solid red line). A similar result can be discerned from the minimum values.

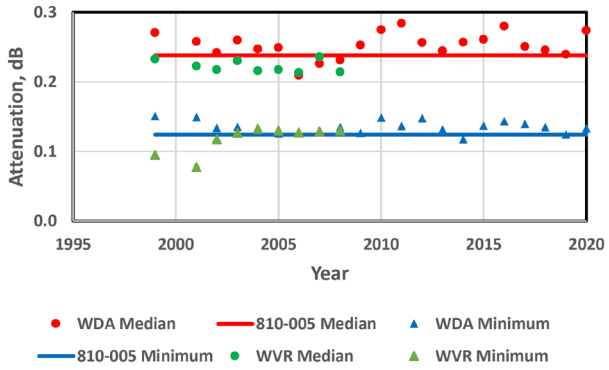

Figure 15. Canberra annual minimum zenith Ka-band atmospheric attenuation measurements derived from WDA (blue triangles), WVR (green triangles), and 810-005 model (solid blue line) and annual median (CD = 50%) zenith Ka-band atmospheric attenuation measurements derived from WDA (red circles), WVR (green circles), and 810-005 model (solid red line).

Figure 16 shows the same type of plot for the atmospheric noise temperatures that were derived from the attenuation values using the formulation described in Section III.D. Here we see generally good agreement with the 810-005 reference curve within ~3 K for the median values and within ~2 K for the minimum values (except for 1999 and 2001). We attribute the differences due to a combination of natural year-to-year variability, model uncertainties, and data selection effects.

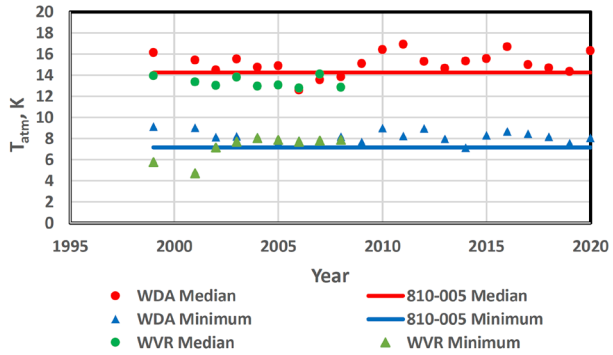

Figure 16. Canberra annual minimum zenith Ka-band atmospheric noise temperature measurements derived from WDA (blue triangles), WVR (green triangles), and 810-005 model (solid blue line), and annual median (CD = 50%) zenith Ka-band atmospheric noise temperature measurements derived from WDA (red circles), WVR (green circles), and 810-005 model (solid red line).

V. Conclusion

We analyzed the statistics from 20 years of WDA data from 2001 to 2021. The statistics were examined for year-to-year consistency and to discern any trends due to calibration issues or natural variability. There was generally reasonable agreement between the WDA data and that of the 810-005 and WVR data for all three sites, where the best agreement was achieved for Madrid. Some anomalies and biases were noted for Goldstone (e.g., minimum values higher than expected for some years) and Canberra (e.g., higher liquid water content than expected). Such data could be used to test and train weather forecast models (such as those used for Ka-band flight operations) in the case that higher quality

data (e.g., AWVR, WVR) are not available. The discrepancies noted can be used in evaluating the error budgets for such data as input to the forecasting algorithms.

Acknowledgments

We acknowledge funding provided by the Research and Technology Development (R&TD) program at the Jet Propulsion Laboratory in Pasadena, California, and Jon Hamkins of the IPN PR. We would like to thank Connie Dang of Peraton, Inc., in Monrovia, California for assistance in obtaining DSN weather data and addressing issues as they arose. We would also like to thank Qing Yue for providing a comprehensive and appreciated review of the paper. The research was carried out at the Jet Propulsion Laboratory, California Institute of Technology, under a contract with the National Aeronautics and Space Administration (80NM0018D0004).

References

[1] S. D. Slobin, "Atmospheric and Environmental Effects," in *DSMS Telecommunications Link Design Handbook,* Doc. 810-005, Module 105, Rev. E, Jet Propulsion Laboratory, California Institute of Technology, Pasadena, California, 2015.

[2] D. D. Morabito, "A comparison of estimates of atmospheric effects on signal propagation using ITU models: Initial study results," *The Interplanetary Network Progress Report,* vol. 42-199, Jet Propulsion Laboratory, Pasadena, California, pp. 1–24, November 15, 2014. http://ipnpr.jpl.nasa.gov/progress_report/42-199/199D.pdf

[3] D. D. Morabito, S. Keihm, and S. Slobin, "A statistical comparison of meteorological data types derived from Deep Space Network water vapor radiometers." *The Interplanetary Network Progress Report,* vol. 42-203, pp. 1–21, Jet Propulsion Laboratory, Pasadena, California, November 15, 2015. https://ipnpr.jpl.nasa.gov/progress_report/42-203/203A.pdf

[4] D. D. Morabito, L. Wu, and S. Slobin, "A comparison of atmospheric quantities determined from advanced WVR and weather analysis data," *The Interplanetary Network Progress Report,* vol. 42-209, pp. 1–12, Jet Propulsion Laboratory, Pasadena, California, May 15, 2017. https://ipnpr.jpl.nasa.gov/progress_report/42-209/209B.pdf

[5] D. D. Morabito, D. Kahan, M. Paik, L. Wu, E. Barbinis, D. Buccino, and M. Parisi, "A study of twenty years of advanced water vapor radiometer data at Goldstone, California," *The Interplanetary Network Progress Report,* vol. 42-228, pp. 1–18, Jet Propulsion Laboratory, Pasadena, California, February 15, 2022. https://ipnpr.jpl.nasa.gov/progress_report/42-228/42-228A.pdf

[6] L. Wu, D. D. Morabito, J. P. Teixeira, L. Huang, H. M. Nguyen, H. Su, M. A. Soriano, L. Pan, and D. S. Kahan, "Prediction of atmospheric noise temperature at the Deep Space Network with machine learning," *Radio Science* 57, e2022RS007483. https://doi.org/10.1029/2022RS007483L

[7] H. Hersbach, B. Bell, P. Berrisford, S. Hirahara, A. Horányi, J. Muñoz-Sabater, J. Nicolas, C. Peubey, R. Radu, D. Schepers, A. Simmons, C. Soci, S. Abdalla, X. Abellan, G. Balsamo, P. Bechtold, G. Biavati, J. Bidlot, M. Bonavita, G. Chiara, P. Dahlgren, D. Dee, M. Diamantakis, R. Dragani, J. Flemming, R. Forbes, M. Fuentes, A. Geer, L. Haimberger, S. Healy, R. J. Hogan, E. Hólm, M. Janisková, S. Keeley, P. Laloyaux, P. Lopez, C. Lupu, G. Radnoti, P. Rosnay, I. Rozum, F. Vamborg, S. Villaume, and J. N. Thépaut, "The ERA5 global reanalysis," *Quarterly Journal of the Royal Meteorological Society* 146, 1999–2049, 2020. https://doi.org/10.1002/qj.3803

[8] D. D. Morabito, "Detection of tropospheric propagation effects from deep space links of the Cassini spacecraft," *Radio Science* 42, RS6007, 2007. http://onlinelibrary.wiley.com/doi/10.1029/2007RS003642/abstract

[9] "Attenuation due to clouds and fog," *Recommendation ITU-R P.840-8*, International Telecommunications Union, Geneva, Switzerland, August 2019

[10] "Specific attenuation model for rain for use in prediction methods," *Recommendation ITU-R P.838-3*, International Telecommunications Union, Geneva, Switzerland, March 2005.

[11] "Method for calculating link performance in the space research service," *Recommendation SA.2183*, International Telecommunications Union, Geneva, Switzerland, October 2010.

[12] "The radio refractive index: Its formula and refractivity data," *Recommendation ITU-R P.453-14*, International Telecommunications Union, Geneva, Switzerland, August 2019.

[13] "Attenuation by atmospheric gases and related effects," *Recommendation P.676-12*, International Telecommunications Union, Geneva, Switzerland, August 2019.

[14] S. D. Slobin, "34-m BWG stations telecommunications interfaces," in *DSMS Telecommunications Link Design Handbook,* Doc. 810-005, Module 104, Rev. O, Jet Propulsion Laboratory, California Institute of Technology, Pasadena, California, 2022.

[15] S. D. Slobin, "Microwave noise temperature and attenuation of clouds: Statistics of these effects at various sites in the United States, Alaska, and Hawaii," *Radio Science* 17(6), 1443–1454, 1982. doi:10.1029/RS017i006p01443.